Journal of Power Sources 196 (2011) 1417–1424

Contents lists available at ScienceDirect

Journal of Power Sources

journal homepage: www.elsevier.com/locate/jpowsour

Electrochemical characterization of electrolytes for lithium-ion batteries based on lithium difluoromono(oxalato)borate

Sandra Zugmann[a], Dominik Moosbauer[a], Marius Amereller[a], Christian Schreiner[a], Franz Wudy[a], René Schmitz[b], Raphael Schmitz[b], Philipp Isken[b], Christian Dippel[b], Romek Müller[b], Miriam Kunze[b], Alexandra Lex-Balducci[b], Martin Winter[b], Heiner Jakob Gores[a,*]

[a] Workgroup "Electrochemistry and Electrolytes", Institute of Physical and Theoretical Chemistry, University of Regensburg, Universtaetsstr. 31, D-93040 Regensburg, Bavaria, Germany
[b] Institute of Physical Chemistry, Westfälische Wilhelms-University Münster, Corrensstraße 28/30, 48149 Münster, Germany

ARTICLE INFO

Article history:
Received 3 May 2010
Received in revised form 28 July 2010
Accepted 10 August 2010
Available online 17 August 2010

Keywords:
Lithium difluoromono(oxalato)borate (LiDFOB)
Hydrolysis
Lithium-ion batteries
Al corrosion
EQCM

ABSTRACT

The salt lithium difluoromono(oxalato)borate (LiDFOB) showed some promising results for lithium-ion-cells. It was synthesized via a new synthetic route that avoids chloride impurities. Here we report the properties of its solutions (solvent blend ethylene carbonate/diethyl carbonate (3:7, mass ratio), including its conductivity, cationic transference number, hydrolysis, Al-current collector corrosion-protection ability and its cycling performance with some electrode materials. Some Al-corrosion studies were also performed with the help of our recently developed computer controlled impedance scanning electrochemical quartz crystal microbalance (EQCM) that proofed to be a useful tool for battery material investigations.

1. Introduction

Electrolytes of lithium-ion batteries (LIBs) are currently mainly based on $LiPF_6$ and blends of organic carbonates such as ethylene carbonate, dimethyl carbonate, diethyl carbonate or propylene carbonate [1,2]. However, $LiPF_6$ has some drawbacks [3], including HF formation with traces of water [4], making the use of cheaper and environmentally more desirable cathode materials such as lithium manganese oxide spinels impossible [5,6]. Its decomposition at rather low temperatures entails the formation of the Lewis acid PF_5 and the scarcely soluble LiF. The Lewis acid PF_5 is able to polymerize solvents [4,7] and thus prevents the use of cationically polymerizable solvents.

Therefore, several years ago, we started the synthesis of lithium chelatoborates [8] and showed what kind of ligands can be used to join the boron atom. The most promising member of the class of lithium salts is lithium bis(oxalato)borate (LiBOB) [9]. It shows better thermal stability and better SEI formation at the Li_xC_6-anode [10] than $LiPF_6$. However, LiBOB also gives a much smaller conductivity in organic carbonates and a reduced solubility at low temperatures, when compared to $LiPF_6$ based solutions. As we knew from other investigations, asymmetric molecular ions increase the solubility of salts, so we tried to synthesize a class of new lithium salts with borates substituted by two different ligands, including semi-chelatoborates. We hoped that the findings of Brownstein and Latremouille [11] that borates with two different monodentate ligands usually equilibrate to equal portions of two borates with the same ligand at the end (e.g. $2[BX_2Y_2]^- \rightarrow [BX_4]^- + [BY_4]^-$) would not be valid for bidentate ligands such as oxalate [12]. Zhang [13] reported a thermal decomposition temperature of about 520 K for lithium difluoromono(oxalato)borate (LiDFOB) synthesized via the etherate-route. He also described some promising results of this salt for its use in lithium-ion-cells.

Ionic liquids (ILs) are currently considered as possible substitutes [14,15] for organic solvents due to their high conductivities and their very low vapor pressures [16], reducing certain safety concerns. We therefore tried to increase the conductivity of our LiDFOB based solutions by adding ILs, too [17]. By this approach, it was possible to largely close the conductivity gap between $LiPF_6$ and LiDFOB based solutions.

For a further characterization of the promising salt LiDFOB and the selected LiDFOB based electrolyte (solvent blend ethylene carbonate/diethyl carbonate (3:7, mass ratio)) we investigated its

* Corresponding author. Tel.: +49 941 943 4746; fax: +49 941 943 4532.
E-mail addresses: heiner.gores@chemie.uni-regensburg.de, w.heitzer_h.j.gores@t-online.de (H.J. Gores).
URL: http://www.electrolytes.de (H.J. Gores).

0378-7753/$ – see front matter © 2010 Elsevier B.V. All rights reserved.
doi:10.1016/j.jpowsour.2010.08.023

conductivity (in comparison with other lithium salts), the hydrolysis of the salt, its thermal stability, its salt diffusion coefficient, and the cationic transference number of the LiDFOB based electrolyte at moderate concentrations by two methods. Electrochemical experiments were performed to determine its behavior during cycling at $LiNi_{1/3}Co_{1/3}Mn_{1/3}O_2$ (NCM) and carbon electrodes. Corrosion studies of aluminum, the current collector for cathode materials, were performed by chronoamperometry and in combination with our recently presented impedance scanning electrochemical quartz crystal microbalance (EQCM) [18]. For comparison, experiments with other lithium salts are reported as well.

2. Experimental

2.1. Materials and equipments

For all measurements the same solvent composition was used: ethylene carbonate (EC) and diethyl carbonate (DEC) (3:7, w/w). EC and DEC were purchased from Merck KGaA, Darmstadt (p.a.). The lithium salts $LiPF_6$ and $LiBF_4$ were purchased from Stella (high purity), lithium trifluoromethylsulfonate (LiOTf) from Merck KGaA, Darmstadt (high purity), bis(trifluoromethansulfonyl) imide (LiTFSI) from 3 M (battery grade, HQ115) and LiBOB from Chemetall, Frankfurt (battery grade). LiDFOB was prepared by the synthesis route introduced by Schreiner et al. [19] resulting in a fine white powder in quantitative yield. Thermal stability measurements were carried out with a Perkin–Elmer Thermogravimetric analyzer (TGA-7).

All solutions were prepared in glove boxes (Mecaplex GB80 or MBRAUN Labmaster DP) with low mass fractions of water ($<1 \times 10^{-6}$) and oxygen ($<5 \times 10^{-6}$). The water content of the electrolytes was $<5 \times 10^{-5}$, checked by Karl Fischer titration (Mettler, type Karl Fischer Titrator DL18). The electrochemical measurements were performed on a Reference 600 potentiostat/galvanostat (Gamry Instruments, USA, Warminster, PA).

$LiNi_{1/3}Co_{1/3}Mn_{1/3}O_2$ (NCM) was provided by Toda Kogyo Europe and used as received. The electrodes containing NCM were prepared using 85% of NCM, 5% Super P (Timcal), 5% Timrex® KS6 (Timcal) and 5% of PVdF (Kynar Flex® 2801, Arkema). The electrode components were mixed in *N*-methyl-pyrrolidon (NMP) and stirred for 1 h. After homogenizing with a dissolver disc for 30 min, the slurry was cast on aluminum foil and dried at 353 K over night. The electrodes were punched from the foil and dried at 393 K in a glass oven (Büchi) over night. The mass loading of the resulting electrodes was about 4 mg cm^{-2} (active mass). The *C*-rate test was done at room temperature between 4.2 and 3.0 V with a constant charge rate of *C*/10 (ca. 0.107 mA cm^{-2}). The discharge rate was varied from *C*/10 (ca. 0.107 mA cm^{-2}) to 5*C* (ca. 5.34 mA cm^{-2}). After the *C*-rate test, constant current–constant voltage (CCCV) tests were carried out between 4.2 and 3.0 V with a current density corresponding to the *C*/2-rate (ca. 0.534 mA cm^{-2}). Both types of measurement were done at 293 ± 2 K with a MACCOR Battery tester Series 4000.

Graphite electrodes were prepared as following: a mixture of 87% of T44 Timrex® graphite (Timcal), 5% Super P (Timcal) and 8% of PVdF (Kynar Flex® 761) was dispersed in *N*,*N*-dimethylformamide (DMF) and homogenized with a dissolver disc for 1 h. The resulting slurry was mixed thoroughly, cast on a copper foil current collector and finally dried in vacuum at 393 K for 24 h. The average mass loading of the active material was about 2.8 mg cm^{-2} for the prepared electrodes. The constant current tests were performed with a MACCOR Battery tester Series 4000 at room temperature. After two initial formation cycles at *C*/5 (ca. 0.157 mA cm^{-2}), the electrodes were cycled at a *C*-rate of *C*/2 (ca. 0.392 mA cm^{-2}).

For measurements with our EQCM, the working electrode, respectively the metallized quartz crystal surface was modified. Pre-tests with commercially available aluminum quartz crystals gave no useful results. The aluminum layer sputtered on the quartz was too thin for usage with more corrosive salts like lithium trifluoromethylsulfonate (LiOTf). After a short time the Al coating was fully dissolved and the underlying chrome metal layer reacts with the electrolyte, leading to further dissolution which finally led to a loss of the electrical contact. In addition to that, measurements with less reactive salts like $LiPF_6$ showed parasitic side reactions, too.

Instead, another method for electrode preparation was used. An adhesive paste (Crystalbond 509, Gatan GmbH, Germany) was dissolved in acetone p.a. and a small amount was dropped on the quartz [20]. After drying at 333 K for 1 h, the quartz was heated up to 400 K. By that, the paste becomes liquid and sticky and a piece of the aluminum foil cut out to the dimensions of the quartz can be glued on the surface. During cooling down to room temperature the foil-quartz assembly was pressed together by a weight.

^{11}B-NMR (128.4 MHz) and ^{19}F-NMR (282.4 MHz) spectra were recorded on a Bruker Avance 400 spectrometer with $BF_3{\cdot}Et_2O$ and $CFCl_3$ as external standards, respectively. The solvent used for hydrolysis measurements was deuteriumoxide (Deutero GmbH, Kastellaun, 99.9% D_2O), mixed with DI water (1:1). The experiment was carried out for 12,000 s at 298 K.

2.2. Conductivity studies

Conductivity measurements were performed with our capillary cells [21], thermostatted with an accuracy of 1 mK in a temperature range of 253–323 K. Compared are the well-known lithium hexafluorophosphate ($LiPF_6$) [2,22] and the three borate salts lithium tetrafluoroborate ($LiBF_4$), lithium difluoromono(oxalato)borate (LiDFOB), and lithium bis(oxalato)borate (LiBOB). The investigated salts were dissolved in a solution of ethylene carbonate (EC)/diethyl carbonate (DEC) (3:7, w/w). The evaluation of the maximum conductivity κ_{max} was realized by non-linear fits to the Casteel–Amis equation [23]:

$$\kappa = \kappa_{max}\left(\frac{m}{\mu}\right)^a \exp\left[b(m-\mu)^2 - \frac{a}{\mu}(m-\mu)\right] \quad (1)$$

with m being the molality (mole per kg solvent) of the electrolyte, μ is the concentration related to κ_{max} as well as a and b fit parameters without physical meaning.

2.3. Transference number measurements

All measurements were done in a thermostatted T-shape glass cell, using a Reference 600 potentiostat (Gamry Instruments). All experiments were carried out in a Faraday-cage to avoid perturbation of very small currents.

Galvanostatic polarization experiments were carried out with current densities ranging from 0.027 to 2.7 mA cm^{-2} and polarization times from 100 to 400 s.

Potentiostatic polarization experiments were done with an applied voltage of 10 mV for 1 h; impedances were measured in the frequency range of 0.1–10,000 Hz.

2.4. Corrosion studies

Two types of corrosion studies were performed, by polarization measurements at Al working electrodes and with the help of our new EQCM.

2.4.1. Polarization measurements

Polarization measurements were carried out with a potentiostat (Solartron SI 1287) using a three electrode cell (Swagelok®). Al foil was used as working electrode and metallic Li for the counter

Table 1
Values of the maximum specific conductivity κ_{max} and the corresponding molal concentration μ of salts in EC/DEC (3:7, w/w) solutions obtained from non-linear fits of conductivity data to the Casteel–Amis equation.

Salt	Temperature (K)	253	293	323
$LiPF_6$	κ_{max} (mS cm^{-1})	2.1100 (±0.0049)	6.2141 (±0.0076)	10.2566 (±0.0062)
	μ (mol kg$^{-1}_{solv}$)	0.69916 (±0.0036)	0.9567 (±0.0031)	1.1178 (±0.0017)
$LiBF_4$	κ_{max} (mS cm^{-1})	0.7658 (±0.0019)	1.9220 (±0.0018)	3.0132 (±0.0027)
	μ (mol kg$^{-1}_{solv}$)	0.7196 (±0.0079)	1.0102 (±0.0038)	1.2297 (±0.0045)
LiDFOB	κ_{max} (mS cm^{-1})	1.57425 (±0.00072)	4.3199 (±0.0010)	7.0680 (±0.0029)
	μ (mol kg$^{-1}_{solv}$)	0.6767 (±0.0011)	0.95449 (±0.00064)	1.1573 (±0.0027)
LiBOB	κ_{max} (mS cm^{-1})	1.3196 (±0.0011)	4.2911 (±0.0045)	7.527 (±0.015)
	μ (mol kg$^{-1}_{solv}$)	0.5001 (±0.0013)	0.7292 (±0.0057)	0.8908 (±0.0093)

and the reference electrodes. The electrolyte solution contained 1 mol L^{-1} LiDFOB in EC/DEC (3:7, w/w). The tests started at open circuit potential (OCP) and then the potential of the working electrodes was increased in steps of 100 mV up to 4.3 V vs. Li/Li$^+$ (potentiodynamic steps). After each potentiodynamic step, the potential was maintained at the reached potential for 1 h (potentiostatic step). During the potentiostatic steps the current associated with the cells was recorded.

2.4.2. EQCM measurements

Corrosion studies were also performed by a combination of cyclic voltammetry (CV) and the quartz crystal microbalance (QCM), resulting in the electrochemical quartz crystal microbalance (EQCM) [18,24]. In these experiments, both current and mass changes are observable. A mathematical expression for the quartz crystal is given by Sauerbrey's law [25]:

$$\Delta f = -\frac{2f_0^2}{A\sqrt{\rho_Q \mu_Q}}\,\Delta m \tag{2}$$

with Δf being the frequency change due to a mass change Δm, f_0 is the resonance frequency, A is the active surface of the quartz, and ρ_Q and μ_Q are the density and shear modulus of the quartz crystal. Mass increase on the quartz surface leads to a shift to lower frequencies.

Cyclic voltammetry measurements using aluminum foil alone gave the same results as the prepared foil-quartz crystal sandwiches, so obviously the electrode surface was not contaminated by the electrode preparation process. EQCM measurements with the foil-quartz crystals showed just some damping of the quartz and an initial frequency shift of f_0 from about 6.0 to 5.5 MHz.

3. Results and discussion

3.1. Conductivity studies

Fig. 1 shows the temperature- and concentration-dependent conductivity of LiDFOB. Table 1 holds the calculated maximum conductivities and the corresponding molal concentrations for all four salts at 253, 293, and 323 K. Table 2 lists the solubilities for the several mixtures.

In summary, $LiPF_6$ gives the best results for conductivity and solubility, but LiDFOB is in favor when only borates are considered. LiDFOB shows a comparably good solubility and a higher specific conductivity than $LiBF_4$, which bears the lowest conductivity of all borates in the studied solvent blend. The solubility decreases with decreasing fluorine content from $LiPF_6$ over $LiBF_4$ to LiDFOB and LiBOB, which shows the lowest solubility. It should be mentioned that the conductivity gap between $LiPF_6$ and LiDFOB based solutions can be reduced by addition of ionic liquids (ILs) [17].

Table 2
Solubilities of some lithium salts (mol kg$^{-1}_{solvent}$) in EC/DEC (3:7, w/w) at room temperature.

$LiPF_6$	$LiBF_4$	LiDFOB	LiBOB
>2.2	1.75	1.4	0.65 (after one week)

3.2. Transference number measurements

The lithium-ion transference number of the LiDFOB based electrolyte was determined by two different methods. First, a combination of DC-polarization and AC-impedance measurements established by Bruce and Vincent [26] was used. Applying a small constant potential to a solution by non-blocking electrodes leads to a decrease of the initial current value until a steady-state value is reached. Because electrode surfaces or resistive layers vary over time, this contribution can be taken into account by impedance measurements shortly before and after potentiostatic polarization [27]. For small polarization potentials (≤10 mV), the steady-state current I_{ss} and initial current I_0 are described by [26]:

$$I_{ss} = \frac{\Delta V}{R_{ss} + (B/t_+\kappa)} \tag{3}$$

and

$$I_0 = \frac{\Delta V}{R_0 + R_e} = \frac{\Delta V}{R_0 + (B/\kappa)} \tag{4}$$

where ΔV is the applied potential, R_e is the electrolyte resistance, R_{ss} and R_0 are the electrode resistances after and before the polarization, respectively, B is the cell constant, κ is the conductivity and t_+ is the cationic transference number.

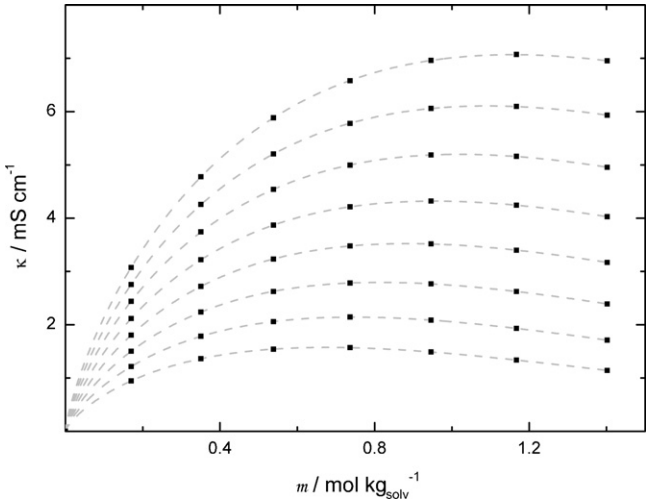

Fig. 1. Temperature-dependent conductivity measurements of LiDFOB in EC/DEC (3:7, w/w), measured data (filled squares) and calculated fits (dashed lines), in 10 K temperature steps from 323 to 253 K, top to bottom.

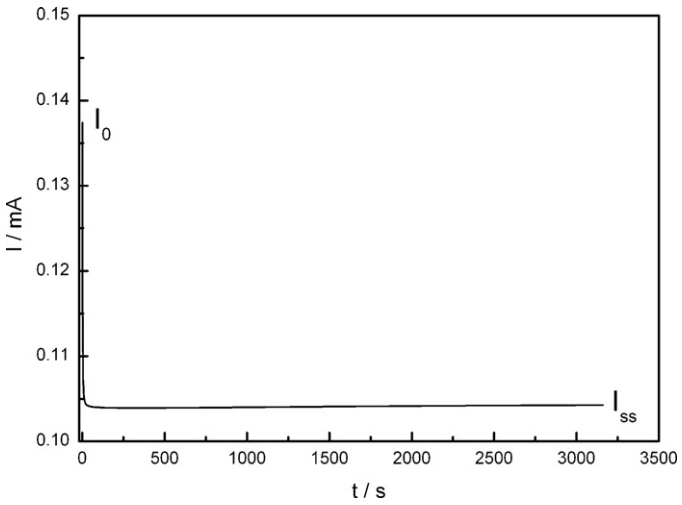

Fig. 2. Chronoamperogram of 0.1 mol kg^{-1} LiDFOB in EC/DEC (3:7, w/w) with an applied voltage of 10 mV. I_0 indicates the initial current, I_{ss} is the steady-state current.

Combining Eq. (3) and (4), the transference number for the cation is given by

$$t_+ = \frac{I_{ss}(\Delta V - I_0 R_0)}{I_0(\Delta V - I_{ss}R_{ss})} \tag{5}$$

The advantage of this method is the rapid procedure, but it is unfortunately underlying some assumptions [26], such as an ideal binary solution.

Fig. 2 shows the steady-state diagram of LiDFOB in EC/DEC (3:7, w/w), 0.1 mol kg^{-1}, where can be seen that the steady-state current I_{ss} is already reached after a short time. Fig. 3 shows the Nyquist plot where the change of the lithium electrode surface during the measurement can be seen. Neglecting this change causes errors that are corrected by determining the electrode resistances before and after the chronoamperometric measurement. The Nyquist plot is fitted to an equivalent circuit [28] representing the electrolyte resistance R_e in series with the two electrodes. The electrode resistances R_0 and R_{ss} are realized by a parallel combination of the lithium-electrolyte interfacial resistances R_1 and R_2 ($(R_1 + R_2)$ is equal to R_0 or R_{ss}) with a constant phase element. The equivalent circuit diagram is shown in Fig. 4.

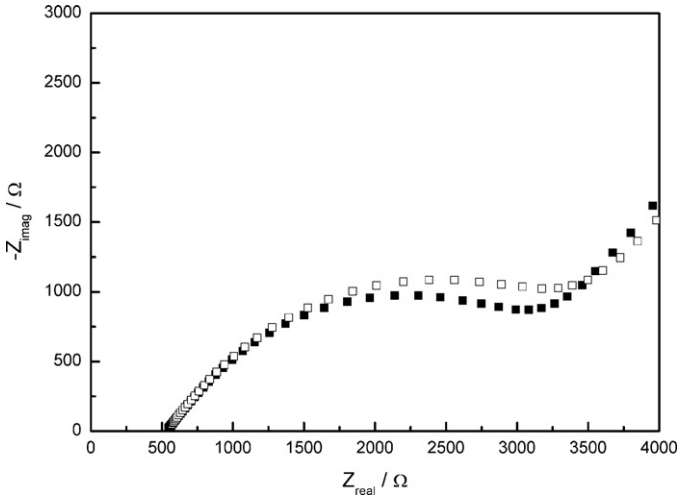

Fig. 3. Nyquist plot of 0.1 mol kg^{-1} LiDFOB in EC/DEC (3:7, w/w). The filled squares show the impedance spectrum before the polarization experiment and the open square after the polarization.

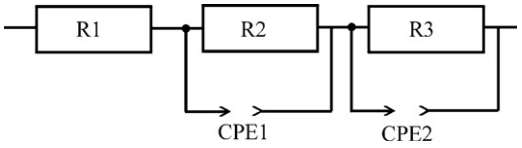

Fig. 4. Equivalent circuit of electrode resistances.

The generally used lithium-electrolyte solution of $LiPF_6$ in ethylene carbonate/dimethyl carbonate/propylene carbonate shows a transference number of 0.38 [22], the determined transference number by the potentiostatic polarization method described in this section for the LiDFOB electrolyte is 0.39 ± 0.005.

The second method used is not restricted to ideal binary solutions and was developed by Newman and co-workers [29]. The concentration gradient is generated by galvanostatic polarization. It is not measured directly but by observing the potential during galvanostatic polarization and determining the exact potential at the moment of current interruption. For the determination of transference numbers, three different measurements are combined: measurement of the potential during galvanostatic polarization, determination of the salt diffusion coefficient, and evaluation of concentration dependence of the cell potential. With these parameters the cationic transference number can be calculated by [30]:

$$t_+ = 1 - \frac{z_+ \nu_+ c_\infty F m \sqrt{D\pi}}{4(dU/d\ln c)} \tag{6}$$

where z_+ is the charge number of the cation, ν_+ is the number of moles of cations added to a solution when one mole of electrolyte is dissolved, c_∞ is the bulk concentration of the salt, D its salt diffusion coefficient, $dU/d\ln c$ the concentration dependence of the potential and m is the slope of a plot of the potential at the time of current interruption vs. $it_i^{0.5}$ where i is the current density and t_i is the polarization time.

This method can be used for non-ideal, concentrated solutions, but some restrictions have to be taken into account, including having a binary electrolyte with the cation as electro-active species, no convection, semi-infinite diffusion and one-dimensional cell geometry.

For determination of the diffusion coefficient, a method developed by Harned and French [31] was used. The negative logarithm of the open circuit potential after a galvanostatic polarization is determined, i.e. the relaxation of a concentration gradient is measured in a vertical closed cell (restricted diffusion). The diffusion coefficient can than be calculated from the slope of the logarithm of the potential difference against time:

$$\ln \Delta U = -\frac{\pi^2 D}{L^2} t + B \tag{7}$$

with L as the electrode distance and the constant B.

The salt diffusion coefficient of 3.95×10^{-10} m^2 s^{-1} was determined by the restricted diffusion method, $dU/d\ln c$ is taken from concentration cell data, measured in a concentration cell without transference.

Fig. 5 shows the negative logarithm of the open circuit potential after galvanostatic polarization, used for the determination of the diffusion coefficient.

Fig. 6 shows the results of the galvanostatic polarization method, leading to a transference number of 0.39 ± 0.03 for LiDFOB in EC/DEC (3:7, w/w), 0.1 mol kg^{-1}, which is in very good agreement with the potentiostatic polarization method.

3.3. Thermal stability

Thermal stability of the solid salt was checked with a Perkin–Elmer Thermogravimetric Analyzer (TGA-7) under a nitro-

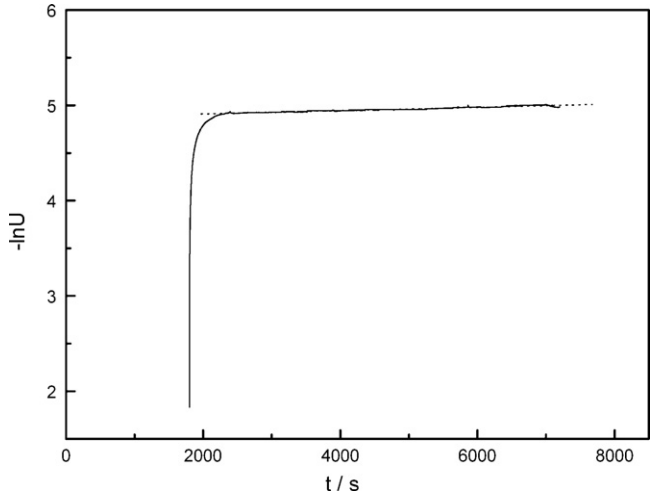

Fig. 5. Plot of the negative logarithm of the open circuit potential U vs. time t after polarization of a 0.1 mol kg^{-1} LiDFOB solution in EC/DEC (3:7, w/w) for the determination of the diffusion coefficient.

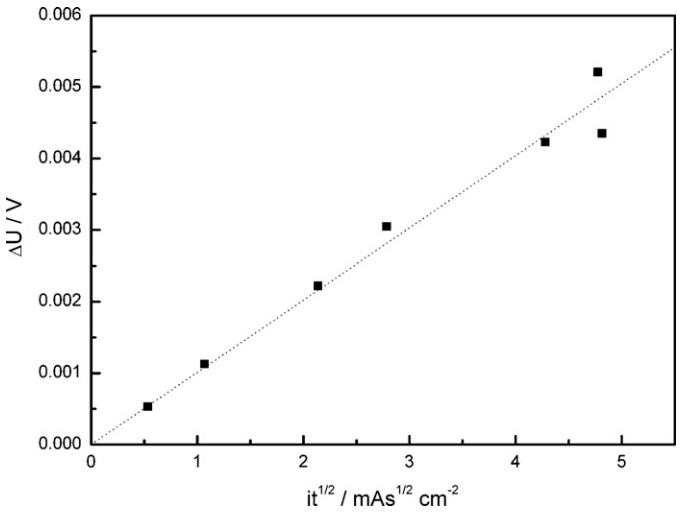

Fig. 6. The determined potential ΔU plotted vs. $it^{1/2}$ for 0.1 mol kg^{-1} LiDFOB in EC/DEC (3:7, w/w).

gen flow at a heating rate of 10 K^{-1}. TGA traces did show that the onset of thermal decomposition of solid LiDFOB is at about 550 K [20], a little bit higher than that reported in the literature [13,32]. To check the long term thermal stability, solid LiDFOB was also stored under Argon at 333 K for 170 days and checked several times by ^{11}B-NMR over this time period. No signs of disproportionation to $LiBF_4$ and LiBOB were detected.

3.4. Hydrolysis

In a previous investigation [33] we have shown that hydrolysis of the DFOB anion in pure water could be studied by conductivity measurements and evaluated according to a pseudo-first order rate law. The rate constants increase with decreasing fluorination of borate anions, $BOB^- > DFOB^- > BF_4^-$. In order to gain more information on produced species, we performed time dependent ^{11}B- and ^{19}F-NMR studies.

The following signals were observed in ^{11}B-NMR spectra during hydrolysis and assigned accordingly as far as possible: 21–17 ppm, very broad, H_3BO_3; 7.4 ppm, singlet, bis(oxalato)borate (BOB^-); 5.2 ppm, broad singlet/doublet, unknown; 4.2 ppm, doublet (13 Hz), $[BF(OH)_3]^-$ (uncertain); 3.5 ppm, singlet, $[BF_2(OH)_2]^-$ (uncertain), 2.7 ppm, singlet, $[DFOB]^-$; 0.1 ppm, quartet (14 Hz), $[BF_3OH]^-$; −1.5 ppm, singlet, $[BF_4]^-$.

The following signals were observed in ^{19}F-NMR spectra during hydrolysis, and assigned accordingly as far as possible: −135.9 ppm, triplet (6 Hz), unknown; −143.9 ppm, quartet (14 Hz), $[BF_3OH]^-$; −148.6 ppm, multiplet, $[BF(OH)_3]^-$ (uncertain); −150.4 ppm, singlet, $[BF_4]^-$; −152.4 ppm, singlet, $[DFOB]^-$.

Figs. 7 and 8a show the time dependency of hydrolysis products as obtained by ^{11}B-NMR.

Fig. 8b shows the results of ^{19}F-NMR-measurements.

It should be stressed that no fluoride (such as HF) was observed in the ^{19}F-NMR spectra. This can be explained by the formation of tetrafluoroborate as one of the main hydrolysis products of the DFOB anion in water, in equilibrium with H_3BO_3 and other borate species.

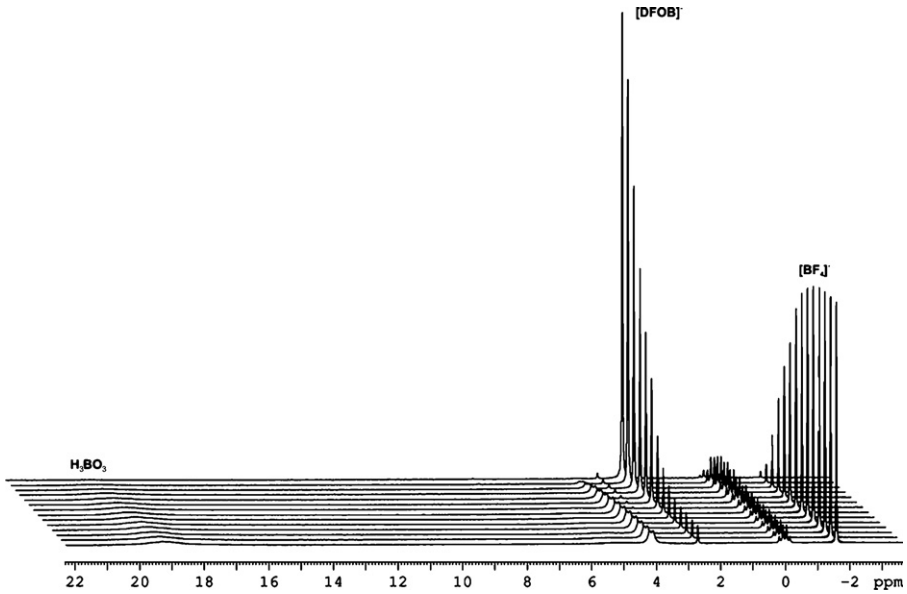

Fig. 7. Stack of all ^{11}B-NMR spectra obtained during the hydrolysis experiment at about room temperature over 24 h. The spectrum in the back is the starting point, the one at the front the end. The z-axis is not scaled.

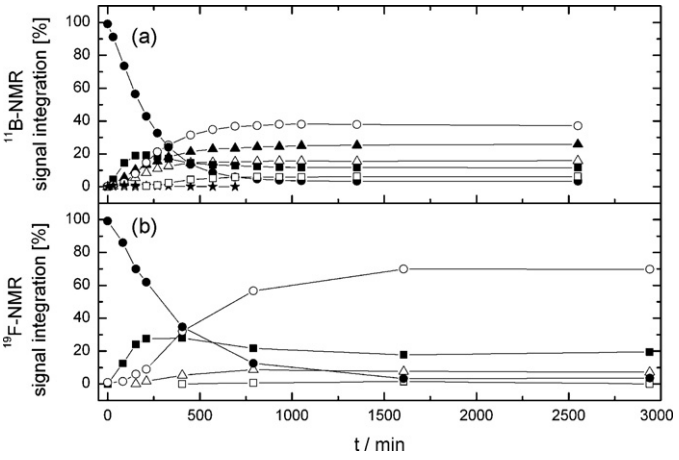

Fig. 8. (a) Relative integration of observed ^{11}B-NMR signals over time during DFOB hydrolysis. (b) Relative integration of observed ^{19}F-NMR signals over time during DFOB hydrolysis. Filled circle: DFOB; open circle: tetrafluoroborate; filled triangle: boric acid; open triangle: monofluorotrihydroxyborate (uncertain); filled square: trifluoromonohydroxyborate; open square: unknown; filled star: difluorodihydroxyborate; open star: bis(oxalato)borate, BOB.

3.5. Corrosion studies

3.5.1. Polarization measurements

Since all investigated electrolyte solutions are electrochemically stable up to the applied upper potential (4.3 V vs. Li/Li$^+$), it is expected that the current will decrease during a potentiostatic step as long as no other Faradaic reactions occur in the system. In contrast, if other types of Faradaic reaction occurred in the system, e.g. corrosion of Al foil, the current would increase over time [34]. Fig. 9 shows the results of this test for the electrolyte LiDFOB in EC/DEC (3:7, w/w). For comparison, the behavior of an electrolyte solution containing the salt lithium bis(trifluoromethylsulfonyl)imide (LiTFSI) with a concentration of 1 mol L^{-1} is reported in the figure, too. LiTFSI is known not to be able to prevent Al corrosion and therefore represents an example where the current increases during the potentiostatic step. As shown in the figure the current density recorded during the potentiostatic step decreases over time for the LiDFOB electrolyte solution, which means that no Faradaic reactions occur up to 4.3 V vs. Li/Li$^+$. Consequently, this electrolyte

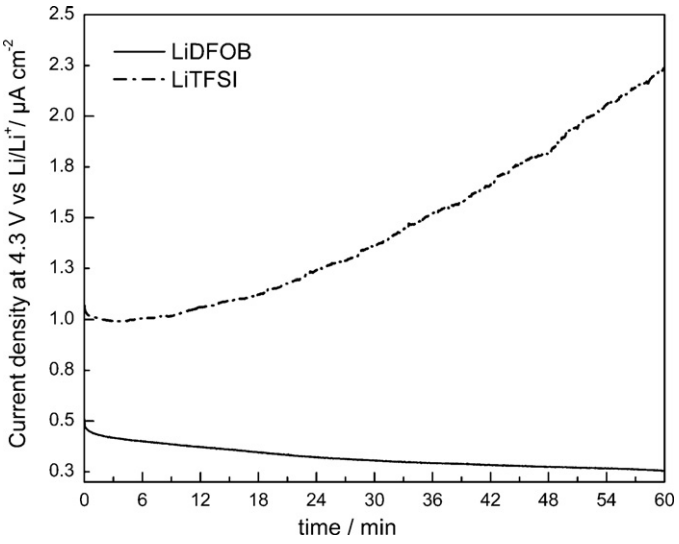

Fig. 9. Corrosion test of an Al collector in a solution containing 1 mol L^{-1} LiDFOB in EC/DEC (3:7, w/w) and 1 mol L^{-1} LiTFSI in EC/DEC (3:7, w/w).

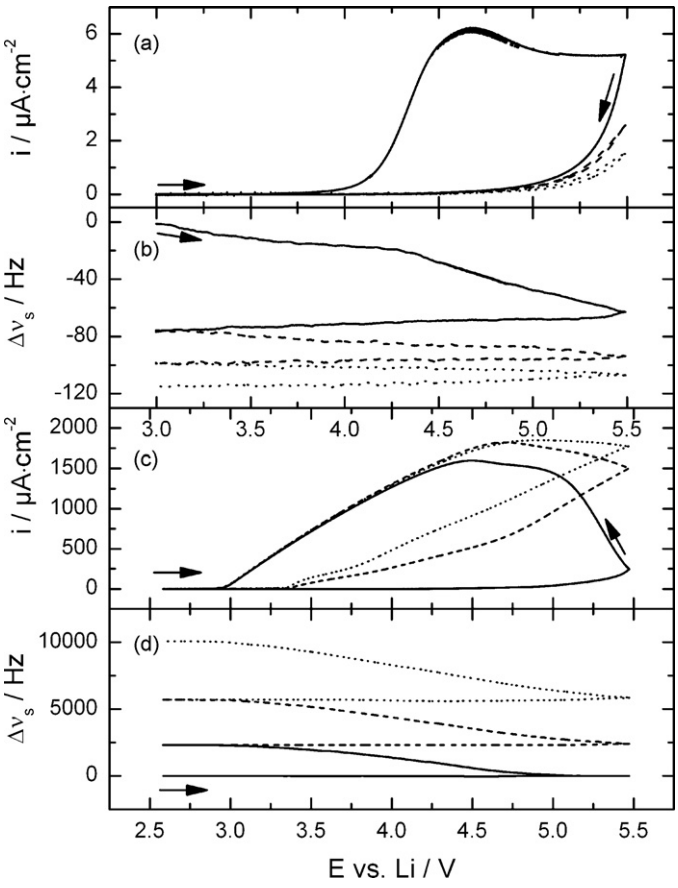

Fig. 10. (a) Cyclic voltammogram, (b) frequency shift, 1 mol L^{-1} LiOTf in EC/DEC (3:7, w/w) on Al-foil quartz. (c) Cyclic voltammogram, (d) frequency shift, 1 mol L^{-1} LiDFOB in EC/DEC (3:7, w/w) on Al-foil quartz, 1st cycle (solid), 2nd cycle (dashed), and 3rd cycle (dotted), $\nu = 5$ mV s^{-1}.

is able to prevent Al corrosion and therefore seems to be a good candidate for usage in contact to battery electrodes at high voltage, too.

3.5.2. EQCM measurements

To prove that the new electrodes (see Section 2.1) are working correctly, LiOTf (known for strong corrosive properties) in addition to LiDFOB was investigated. Fig. 10a shows the corrosion behavior of a LiOTf solution on aluminum foil-quartz crystals. The first cycle shows in its back scan a strong increase of the current due to electrolyte decomposition, consecutive corrosion, and dissolution of aluminum. The following cycles already show aluminum dissolution beginning from 3.3 V vs. Li/Li$^+$ on. Fig. 10b displays the change of the frequency. With every cycle the frequency increases, from 2300 Hz after the first cycle to >10000 Hz after the third cycle. This increase is associated with a significant loss of mass, i.e. the aluminum corrodes and is getting dissolved.

In contrast, $LiPF_6$ is known for its very efficient passivation behavior [35]. An interesting alternative for $LiPF_6$ which is known for its low thermal stability [36], is LiDFOB [12]. Compared to $LiPF_6$, electrolyte decomposition occurs at about 0.5 V higher voltages (at ca. 4.0 V vs. Li/Li$^+$) (see Fig. 10c). After passivation, electrolyte decomposition is observed at about 5 V vs. Li/Li$^+$. The EQCM records a continuous decrease of the frequency with the biggest drop for the first cycle, as seen in Fig. 10d. This indicates an increase in mass due to the deposition of a protecting layer on the aluminum surface.

The measurements above show that LiDFOB is a very promising salt for practical use in lithium-ion batteries concerning the corrosion of the current collector. Furthermore, the method with the

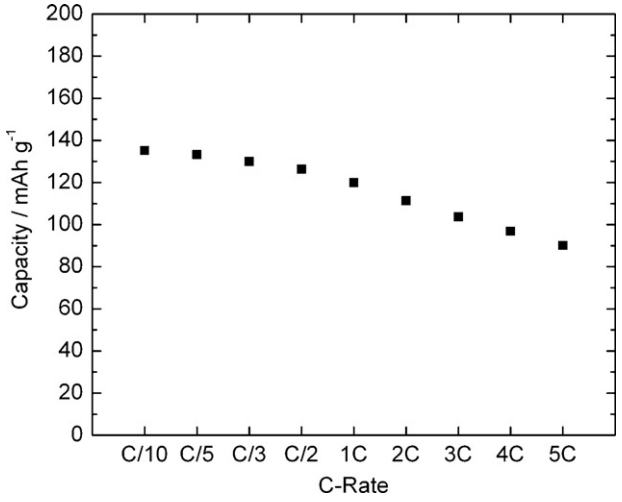

Fig. 11. Rate performance of NCM-based electrodes in a solution of 1 mol L^{-1} LiDFOB in EC/DEC (3:7, w/w).

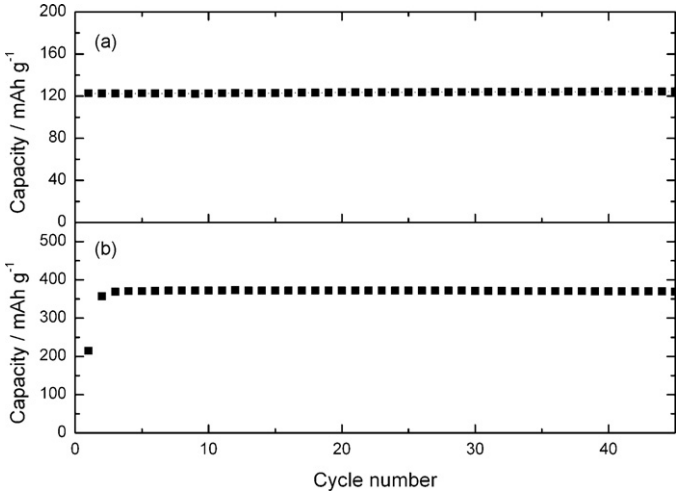

Fig. 12. (a) Cycling performance of NCM electrode in a solution of 1 mol L^{-1} LiDFOB in EC/DEC (3:7, w/w) recorded at RT and *C*/2-rate. (b) Cycling performance of a T44 graphite electrode recorded at RT and *C*/2-rate (the first two cycles were carried out at *C*/5).

foil-quartz assembly is a practical way to combine two techniques, electrochemical methods with the QCM.

3.6. Cycling behavior at electrode materials

A solution of 1 mol L^{-1} LiDFOB in EC/DEC (3:7, w/w) was used in combination with electrodes containing NCM and graphite T44 as active materials. The electrodes were prepared as reported in Section 2 and tested at room temperature. Fig. 11 shows the results relative to the NCM-based electrodes. It reports the results of the *C*-rate tests carried out in the potential range between 3.0 and 4.2 V vs. Li/Li^+. As shown in this figure, the discharge capacity of the electrodes depends on the discharge rate. At a *C*-rate of *C*/10, the electrode shows a specific capacity of around 140 mAh g^{-1}, in good agreement with previously reported values in the literature for this material, when charged to the same upper potential as here (4.2 V vs. Li/Li^+) [37–39]. When the discharge rate is increased, the specific capacity constantly decreases to a value of about 90 mAh g^{-1} for a *C*-rate of 5*C*. After the *C*-rate tests, constant current–constant voltage (CCCV) tests were carried out with a current density corresponding to *C*/2. The results are reported in Fig. 12a. The electrode gave a specific discharge value of about 120 mAh g^{-1}, in good agreement with the value obtained during the power rate test at the same discharge rate. As shown in the figure, the discharge capacity was constant for 50 cycles indicating that electrodes based on NCM used in combination with electrolytes containing the salt LiDFOB are able to provide very high capacity retention and high performance at relative high *C*-rates.

Additionally, the electrolyte solution of 1 mol L^{-1} LiDFOB in EC/DEC (3:7, w/w) was investigated in combination with electrodes based on graphite T44. After two formation cycles at *C*/5 the electrode was charged/discharged at a *C*-rate of *C*/2 at RT. The results of these tests are reported in Fig. 12b. As shown in the figure, the system displays a low value for the specific capacity (ca. 215 mAh g^{-1}) at the first cycle. The efficiency of the first cycle was only 42%, indicating the presence of a high irreversible capacity loss during the SEI-formation process. However, starting from the second cycle, the specific capacity of the electrode increased and reached a constant value of about 370 mAh g^{-1} for 50 cycles. This specific capacity can certainly be considered as very interesting and this result seems to indicate that the electrolyte solution of 1 mol L^{-1} LiDFOB in EC/DEC (3:7, w/w) displays a good affinity to the graphite electrodes. It is important to note that no additives were used for the electrolyte solution; therefore it is reasonable to assume that the addition of an additive to the electrolyte, e.g. vinyl chloride (VC) could reduce the irreversible capacity loss at the first cycle and further improve the already promising electrode performance.

4. Conclusion

The salt lithium difluoromono(oxalato)borate (LiDFOB) shows several very interesting properties for its use in lithium-ion batteries including excellent Al-corrosion-protection properties, excellent cycling behavior of lithiated carbon anodes and $LiNi_{1/3}Co_{1/3}Mn_{1/3}O_2$ (NCM) cathodes, no HF-evaluation upon hydrolysis, and far better solubility when compared to lithium bis(oxalate)borate (LiBOB). Our recently developed computer controlled impedance scanning electrochemical quartz crystal microbalance (EQCM) proofed to be a useful tool for aluminum corrosion studies.

Acknowledgements

Financial support from the German Research Foundation (DFG), contract numbers 544243 and 544241, Project Initiative PAK 177 “Funktionsmaterialien und Materialanalytik zu Lithium-Hochleistungsbatterien” is gratefully acknowledged.

Parts of this paper were recently presented by the corresponding author as a talk given at the HDT-Meeting (Kraftwerk Batterie), Mainz, Germany, February 1st, 2010.

References

[1] M. Schmidt, U. Heider, A. Kuehner, R. Oesten, M. Jungnitz, N. Ignat'ev, P. Sartori, J. Power Sources 97–98 (2001) 557–560.
[2] M.S. Ding, J. Electrochem. Soc. 150 (2003) A620–A628.
[3] J.-I. Yamaki, in: W. Von Schalkwijk, B. Scrosati (Eds.), Advances in Lithium-Ion Batteries, Kluwer Academic, New York, 2002.
[4] S.E. Sloop, J.K. Pugh, S. Wang, J.B. Kerr, K. Kinoshita, Electrochem. Solid-State Lett. 4 (2001) A42–A44.
[5] M.M. Thackeray, Prog. Solid State Chem. 25 (1997) 1–71.
[6] M.S. Whittingham, Chem. Rev. 104 (2004) 4271–4301.
[7] A.M. Andersson, K. Edstrom, J. Electrochem. Soc. 148 (2001) A1100–A1109.
[8] J. Barthel, H.J. Gores, Liquid nonaqueous electrolytes, in: J.O. Besenhard (Ed.), Handbook of Battery Materials, VCH, New York pp. 457–497, (1999); new edition in preparation, Ed.: C. Daniel.
[9] W. Xu, A.J. Shusterman, M. Videa, V. Velikov, R. Marzke, C.A. Angell, J. Electrochem. Soc. 150 (2003) E74–E80.
[10] K. Xu, Chem. Rev. 104 (2004) 4303–4418.
[11] S. Brownstein, G. Latremouille, Can. J. Chem. 56 (1978) 2764.

[12] C. Schreiner, Synthese und Charakterisierung neuer Ionischer Flüssigkeiten auf der Basis gemischter Fluoroborat-Anionen, Dissertation, University Regensburg, 2009.
[13] S.S. Zhang, Electrochem. Commun. 8 (2006) 1423–1428.
[14] H. Sakaebe, H. Matsumoto, Electrochem. Commun. 5 (2003) 594–598.
[15] R. Hagiwara, Y. Ito, J. Fluorine Chem. 105 (2000) 221–227.
[16] M. Galinski, A. Lewandowski, I. Stepniak, Electrochim. Acta 51 (2006) 5567–5580.
[17] D. Moosbauer, S. Zugmann, M. Amereller, H.J. Gores, J. Chem. Eng. Data 55 (2010) 1794–1798.
[18] F. Wudy, M. Multerer, C. Stock, G. Schmeer, H.J. Gores, Electrochim. Acta 53 (2008) 6568–6574.
[19] C. Schreiner, M. Amereller, H.J. Gores, Chem. Eur. J. 15 (2009) 2270–2272.
[20] R.V. Bucur, J.O. Carlsson, V.M. Mecea, Sens. Actuators B 37 (1996) 91–95.
[21] E. Carl, Neue Elektrolyte in organischen Carbonatloesungen zur Anwendung in sekundaeren Lithium-Ionen-Batterien, Dissertation, University Regensburg, 1998.
[22] L.O. Valoen, J.N. Reimers, J. Electrochem. Soc. 152 (2005) A882–A891.
[23] J.F. Casteel, E.S. Amis, J. Chem. Eng. Data 17 (1972) 55–59.
[24] F. Wudy, C. Stock, H.J. Gores, Encyclopedia of Electrochemical Power Sources, Elsevier, 2009.
[25] G. Sauerbrey, Z. Phys. A: Hadrons Nucl. 155 (1959) 206–222.
[26] P.G. Bruce, C.A. Vincent, J. Electroanal. Chem. 225 (1987) 1–17.
[27] J. Evans, C.A. Vincent, P.G. Bruce, Polymer 28 (1987) 2324–2328.
[28] M. Riley, P.S. Fedkiw, S.A. Khan, J. Electrochem. Soc. 149 (2002) A667–A674.
[29] Y. Ma, M. Doyle, T.F. Fuller, M.M. Doeff, L.C. De Jonghe, J. Newman, J. Electrochem. Soc. 142 (1995) 1859–1868.
[30] H. Hafezi, J. Newman, J. Electrochem. Soc. 147 (2000) 3036–3042.
[31] H. Harned, D.M. French, Ann. N. Y. Acad. Sci. 46 (1945) 267–284.
[32] S.S. Zhang, K. Xu, T.R. Jow, J. Power Sources 159 (2006) 702–707.
[33] M. Amereller, M. Multerer, C. Schreiner, J. Lodermeyer, A. Schmid, J. Barthel, H.J. Gores, J. Chem. Eng. Data 54 (2009) 468–471.
[34] A. Lex-Balducci, R. Schmitz, R. Schmitz, R. Müller, M. Amereller, D. Moosbauer, H.J. Gores, M. Winter, ECS Transactions 25(36, Rechargeable Lithium-Ion Batteries) (2010) 13–17.
[35] X. Zhang, B. Winget, M.M. Doeff, J. Evans, T.M. Devine, J. Electrochem. Soc. 152 (2005) B448–B454.
[36] T. Kawamura, A. Kimura, M. Egashira, S. Okada, J.-I. Yamaki, J. Power Sources 104 (2002) 260–264.
[37] H.-S. Kim, S.-I. Kim, C.-W. Lee, S.-I. Moon, J. Electroceram. 17 (2006) 673–677.
[38] J. Choi, A. Manthiram, J. Electrochem. Soc. 152 (2005) A1714–A1717.
[39] P. He, H. Wang, L. Qi, T. Osaka, J. Power Sources 160 (2006) 627–632.